

A Competitive Deep Neural Network Approach for the ImageCLEFmed Caption 2020 Task

Marimuthu Kalimuthu, Fabrizio Nunnari, and Daniel Sonntag

German Research Center for Artificial Intelligence (DFKI)
 Saarland Informatics Campus, 66123 Saarbrücken, Germany
 {marimuthu.kalimuthu,fabrizio.nunnari,daniel.sonntag}@dfki.de

Abstract. The aim of ImageCLEFmed Caption task is to develop a system that automatically labels radiology images with relevant medical concepts. We describe our Deep Neural Network (DNN) based approach for tackling this problem. On the challenge test set of 3,534 radiology images, our system achieves an F1 score of 0.375 and ranks high, 12th among all systems that were successfully submitted to the challenge, whereby we only rely on the provided data sources and do not use any external medical knowledge or ontologies, or pretrained models from other medical image repositories or application domains.

Keywords: Medical Imaging, Concept Detection, Image Labeling, Multi-Label Classification, Deep Convolutional Neural Networks.

1 Introduction

ImageCLEF organises 4 main tasks for the 2020 edition with a global objective of promoting the evaluation of technologies for annotation, indexing, and retrieval of visual data with the aim of providing information access to large collections of images in various usage scenarios and application domains, including medicine [4].

Interpreting and summarizing the insights gained from medical images is a time-consuming task that involves highly trained experts and often represents a bottleneck in clinical diagnosis pipelines. Consequently, there is a considerable need for automatic methods that can approximate this mapping from visual information to condensed textual descriptions. The more image characteristics are known, the more structured are the radiology scans and hence, the more efficient are the radiologists regarding interpretation, see <https://www.imageclef.org/2020/medical/caption/> and [11].

Recent years have witnessed tremendous advances in deep neural networks in terms of architectures, optimization algorithms, tooling and techniques for training large networks, and handling multiple modalities (e.g., text, images, videos,

Copyright © 2020 for this paper by its authors. Use permitted under Creative Commons License Attribution 4.0 International (CC BY 4.0). CLEF 2020, 22-25 September 2020, Thessaloniki, Greece.

speech, etc.). In particular, deep convolutional neural networks have proved to be extremely successful image encoders and have thus become the de facto standard for visual recognition [2,3,13]. We have been working on machine learning problems in several medical application domains [14,15,16,17] in our projects, see <https://ai-in-medicine.dfgi.de/>. In this paper, we describe how we built a competitive deep neural network approach based on these projects.

The rest of the paper is organized as follows. In Section 2, we formally describe the challenge and its goal. In Section 3, we present some statistics on the dataset and explain the approach we adopted to tackle the challenge. In Section 4, we describe the experiments that we conducted with different architectures and introduce a new loss function that addresses the sparsity problem in ground truth labels. In Section 5, results are presented followed by a short discussion. Finally, we summarize our paper in Section 6 and discuss some future directions.

2 The Challenge

The overarching goal of ImageCLEFmed Caption challenge is to assist medical experts such as radiologists in interpreting and summarising information contained in medical images. As a first step towards this goal, a simpler task would be to detect as many key concepts as possible, with the goal that these concepts can then be composed into comprehensible sentences, and eventually into medical reports. For full details about the challenge, we refer the reader to Pelka et al. [11].

The challenge has evolved over the years, since its first edition in 2017, to focus only on radiology images in this year’s version, and incorporating the lessons learned from previous years. The aim of 2020 ImageCLEFmed Caption challenge is to develop a system that would automatically assign medical concepts to radiology images that were sorted into 7 different categories (see Table 1). More concretely, given an image (\mathcal{I}), the objective is to learn a function \mathcal{F} that maps \mathcal{I} to a set of concepts ($\mathcal{C}_1, \mathcal{C}_2, \dots, \mathcal{C}_v$) where v is the number of concepts associated with \mathcal{I} . A peculiarity of this challenge is that $v \ll k$, where k is the total number of unique labels.

$$\mathcal{F} : \mathcal{I} \rightarrow (\mathcal{C}_1, \mathcal{C}_2, \dots, \mathcal{C}_v)$$

On the challenge data, the ground truth concepts are not known for images in the test set. The only known constraint is that predictions of the test set must be submitted with a maximum of 100 non-repeating concepts per image.

The performance of submissions to the challenge are evaluated on a withheld test set of 3,534 images using the *F1* score evaluation metric, which is defined as the harmonic mean of *precision* and *recall* values.

$$F1 = 2 * \frac{precision * recall}{precision + recall}$$

Firstly, the instance level F1 scores are computed using the *predicted* concepts for images in the test set. Later, an average F1 score is computed over all images in the test set using scikit-learn¹ library’s default *binary* averaging method. This yields the final F1 score for an accepted submission.

All registered teams are allowed for a maximum of 10 submissions. Successful submissions and teams are then ranked based on the achieved F1 scores and results are made publicly available.

3 Method

We provide information about the dataset and some analysis that we performed on it during the exploratory phase. Then, we discuss our learning approach and a suitable data preparation strategy.

3.1 Dataset

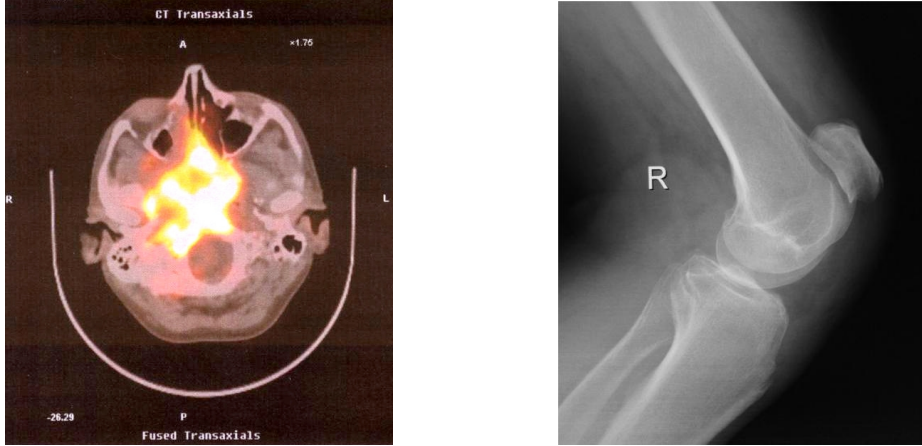
All participants are provided with *ImageCLEFmed Caption* dataset which is a subset of the ROCO dataset [12]. It is a multi-modal, medical images dataset containing radiology images that are labelled with a set of medical concepts, called as Concept Unique Identifiers (CUIs) in the literature. As common in many challenges, the provided images are already split into *Train*, *Validation*, and *Test* sets. Images of the first two sets come with ground truth labels, while the *test* set contains only images.

Abbreviation	Full form
DRAN	DR Angiography
DRCO	DR Combined modalities in One image
DRCT	DR Computerized Tomography
DRMR	DR Magenetic Resonance
DRPE	DR Positron Emission Tomography
DRUS	DR Ultrasound
DRXR	DR X-Ray, 2D Tomography

Table 1: Terminology used in “ROCO” dataset.

Moreover, images in each of the splits are sorted into one of the 7 categories as described in tables 1 and 2; such information can be inferred from the name of the sub-directory containing the images. As we can observe from Table 2, the images are not equally distributed across categories, indicating an imbalance in the dataset. The DRCT category, which contains images captured using Computerized Tomography (CT), has the highest representation, followed by X-ray

¹https://scikit-learn.org/stable/modules/generated/sklearn.metrics.f1_score.html



CUI	UMLS Term (Concept)
C2951888	set of bones of skull
C0037303	set of bones of cranium
C0032743	tomogr positron emission
C0342952	increased basal metabolic rate

CUI	UMLS Term
C0022742	knees
C0043299	x-ray procedure
C1260920	kneel
C0030647	bone, patella

Fig. 1: Sample images & their CUIs from the *train* split.

images (DRXR), while the least number of images (approximately $\frac{1}{40}$ th of the images in DRCT) are seen in DRCO category.

Split	Total Number of Images in the Category of							Total
	DRAN	DRCO	DRCT	DRMR	DRPE	DRUS	DRXR	
Train	4,713	487	20,031	11,447	502	8,629	18,944	64,753
Val	1,132	73	4,992	2,848	74	2,134	4,717	15,970
Test	325	49	1,140	562	38	502	918	3,354

Table 2: Splits and statistics of ImageCLEFmed Caption dataset.

Despite having these *category* labels as a meta-information, we could not leverage them during model training due to time constraints. Thus, the relationship between CUIs and image category labels is, for us, still uninvestigated. Possibly, in a follow-up work we will investigate on how to exploit such meta-information to improve classification performance of predictive models, for example by using one of the metadata fusion strategies tested by the authors in [9].

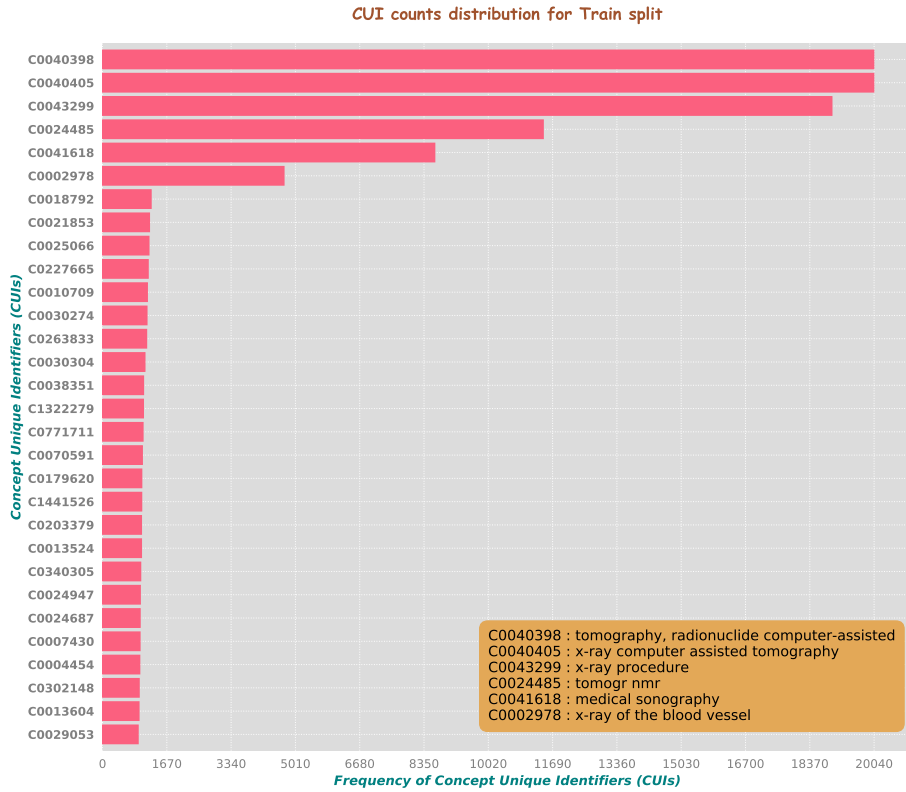


Fig. 2: Histogram of top 30 CUIs on the *training* split.

3.2 Data Analysis

Here, we outline some insights that we gained after performing analysis on the CUIs and the category labels meta-information. Furthermore, this section sheds light on the imbalance in the dataset, which is a common problem in many research domains.

Figure 1 provides a conceptual representation of the input, viz. images paired with relevant concepts. In this case, both images are labelled with four CUIs, the descriptions of which are provided by Unified Medical Language System (UMLS)² terms. These terms are depicted in Figure 1 merely for the purpose of understanding since the mapping of CUIs to UMLS terms is not part of the provided dataset.

Figure 2 shows the frequencies of top 30 CUIs on the training split. Two CUIs (*C0040398*, *C0040405*), which both occur around 20k times in the training set, dominate this list and represent the concept “computer assisted tomography”.

²<https://www.nlm.nih.gov/research/umls/>

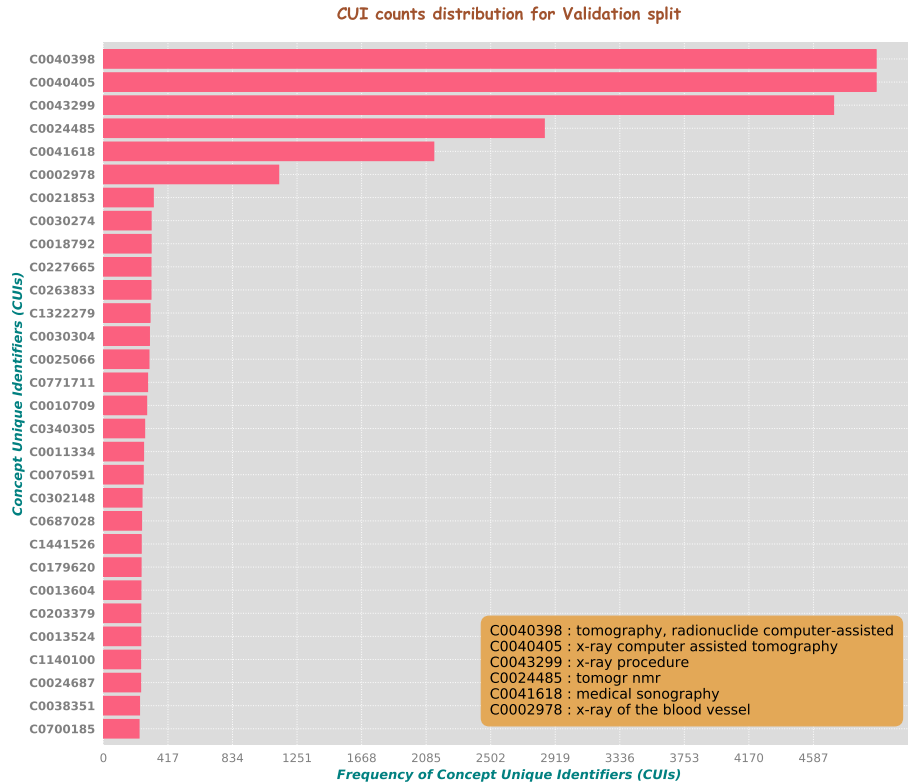


Fig. 3: Histogram of top 30 CUIs on the *validation* split.

Similar behavior is observed on the validation set (see Figure 3). However, the frequencies of top 2 CUIs in this case are only around 4.6k.

Figure 4 depicts a histogram representation of the number of images and the CUI counts on the training set. For instance, there are around 5,200 images that have exactly two CUIs as ground truth labels. On the contrary, there are only around 100 images that have exactly 50 CUIs as ground truth labels in the provided training set. This histogram is truncated at CUI count 50 (x-axis) for clarity and uncluttered representation.

In a similar manner, Figure 5 shows a histogram representation of the number of images and the CUI counts on the validation set. For instance, there are around 1,300 images that have exactly two CUIs as ground truth labels. On the contrary, there are only around 30 images that have exactly 50 CUIs as ground truth labels in the validation set. This histogram is truncated at CUI count 50 (x-axis) for clarity and uncluttered representation.

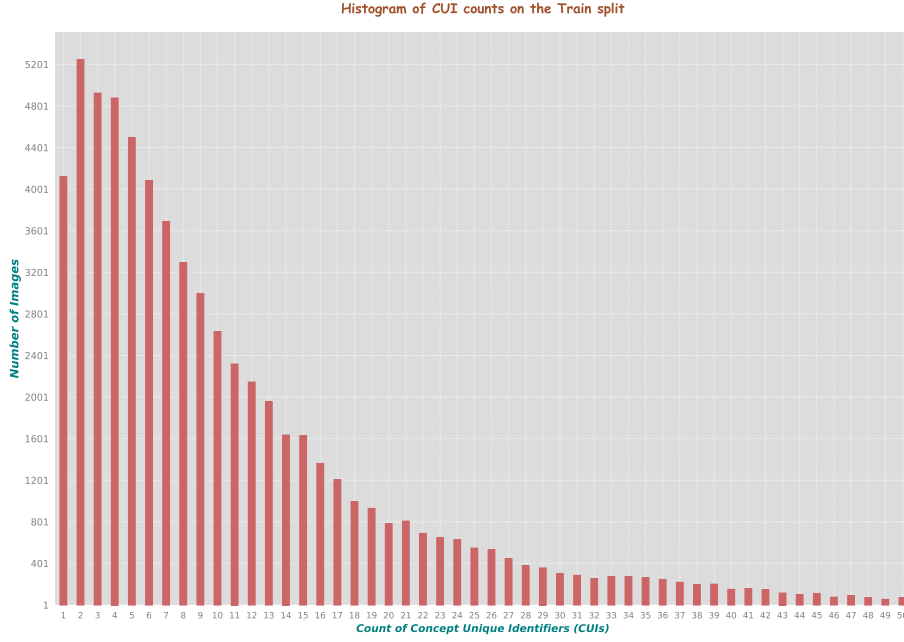


Fig. 4: Histogram of CUI counts vs. Images Count on the *training* set after combining all of the 7 categories.

On the combined training and validation set, there are 80,723 images and 907,718 non-unique CUIs. Among them, we counted 3,047 unique CUIs, which were used to build our *label space* in our training objective (see Table 3).

Following Tsoumakas et al. [18], we compute the *Label Cardinality* (LC) on the combined training and validation set, denoted as \mathcal{D} , using the formula:

$$LC(\mathcal{D}) = \frac{1}{|\mathcal{D}|} \sum_{i=1}^{|\mathcal{D}|} |Y_i|$$

In a similar manner, we compute the *Label Density* (LD) using the following formula:

$$LD(\mathcal{D}) = \frac{1}{|\mathcal{D}|} \sum_{i=1}^{|\mathcal{D}|} \frac{|Y_i|}{|L|}$$

where $|L|$ is the number of unique labels in our multi-label classification objective. The LC and LD scores on the combined training and validation sets are 11.24 and 0.0037 respectively.

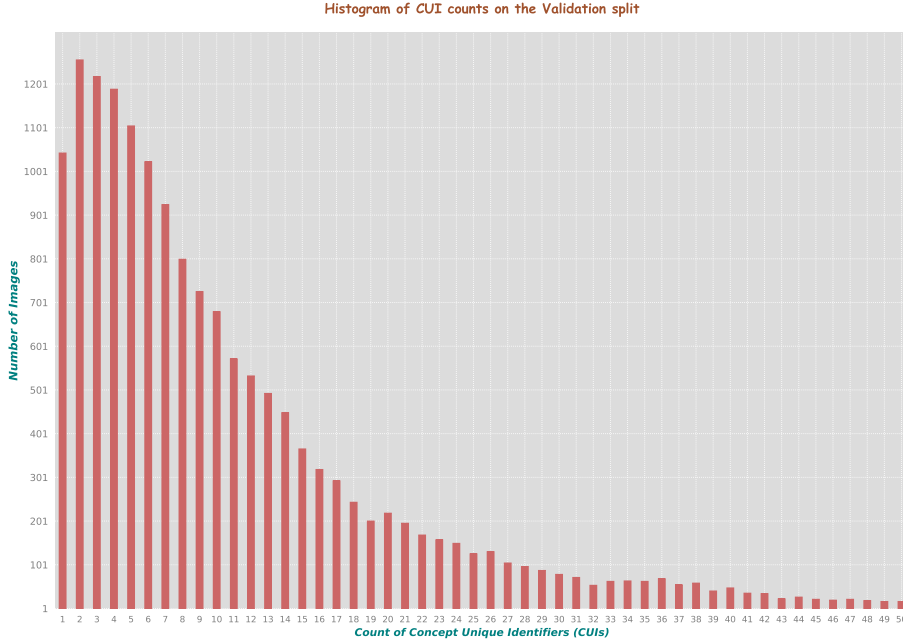


Fig. 5: Histogram of CUI counts vs. Images Count on the *validation* set after combining all of the 7 categories.

3.3 Data preparation

As a first step in formatting the labels, we convert CUIs associated with images to a format that is suitable as input for neural network learning. Since our objective here is *multi-label* classification, we cannot use simple *one-hot* encoding, as usually done in classification tasks, hence we apply a *multi one-hot* encoding. An illustration of this representation is found in Table 3. Specifically, we sort the list of CUIs from the unique label set (k) in alphabetical order and use the positions of CUIs in the sorted list to mark as 1 if a specific CUI is associated with the image in question, else as 0. After this conversion step, the label set for each image (\mathcal{I}) is represented as a single *multi one-hot* vector of fixed size k , which is equal to 3,047.

We used only the images from ImageCLEFmed Caption dataset and did not use pre-training on external datasets, or utilize other modalities such as text during model training.

For our experiments, we divided the validation set via random sampling into two equally sized subsets, namely $val1$ and $val2$. We conducted our internal evaluations by always training pairs of models, first using $val1$ for validation and $val2$ for testing, and then vice-versa. When results were promising, we then submitted our predictions on the test set images by using the model trained with first configuration. Training a third model, based on the validation on the full

Image	Multi One-Hot Encoding
	CUI01, CUI02, CUI03, ..., CUI3047
<i>ROCO2_CLEF_76012.jpg</i>	...,0,1,0,0,1,0,0,0,1...
<i>ROCO2_CLEF_05856.jpg</i>	...,0,0,0,0,0,0,0,0,1...
<i>ROCO2_CLEF_45763.jpg</i>	...,0,1,0,0,1,0,1,0,0...
:	:

Table 3: Encoding CUIs using *multi one-hot* representation.

development set would have been the ideal solution. However, this could not be applied in our case because of time constraints.

3.4 Learning Approach

The prediction problem for this challenge lays in the category of *multi-label classification* [18]. It differs from most common classification problems in the fact that each sample of the dataset is simultaneously associated with more than one class from the ground truth label pool.

Technically, when addressing such a problem with deep neural networks, it means that the final classification layer relies on multiple sigmoidal units rather than a single softmax probability distribution. The last layer of the network contains one sigmoidal unit for each of the target classes, and the association with a true/false result is performed by thresholding the final sigmoid activation value (usually at 0.5).

To address the challenge, we followed a classical transfer learning approach starting from a Convolutional Neural Network (CNN) model pre-trained on an image classification problem, namely ImageNet, because the pre-trained network already offers the ability to detect basic image features, viz. edges, borders, and corners. Then, the final classification stage of the network (i.e., all the layers after the last convolutional layer) is substituted with randomly initialized fully connected layers. Finally, the network is fitted for the new target training set.

In detail, we used VGG16 [13], ResNet50 [2], and DenseNet169 [3], all of them pre-trained on ImageNet data used for ILSVRC [6]. An example configuration based on VGG16 is shown in listing 1.1. Layers from `block1_conv1` to `block5_pool` are pre-trained on ImageNet, and unlocked for further training. Remaining layers, from `flatten` to `predictions`, are newly instantiated and initialized randomly (where applicable). The final `predictions` layer is a dense layer with 3,047 sigmoidal activation units (one per target class).

The system was developed in a Python environment using Keras deep learning framework [1] with TensorFlow [7] as the backend. For our experiments we used a desktop machine equipped with an 8-core 9th-gen i7 CPU, 64GB RAM, and NVIDIA RTX TITAN 24GB GPU memory.

1	Layer (type)	Output Shape	Param #	
2	<hr/>			
3	input_1 (InputLayer)	(None, 227, 227, 3)	0	
4	<hr/>			
5	block1_conv1 (Conv2D)	(None, 227, 227, 64)	1792	
6	<hr/>			
7	block1_conv2 (Conv2D)	(None, 227, 227, 64)	36928	
8	<hr/>			
9	block1_pool (MaxPooling2D)	(None, 113, 113, 64)	0	
10	<hr/>			
11	[... 13 more layers ...]			
12	<hr/>			
13	block5_conv3 (Conv2D)	(None, 14, 14, 512)	2359808	
14	<hr/>			
15	block5_pool (MaxPooling2D)	(None, 7, 7, 512)	0	
16	<hr/>			
17	flatten (Flatten)	(None, 25088)	0	
18	<hr/>			
19	fc1 (Dense)	(None, 4096)	102764544	
20	<hr/>			
21	dropout_1 (Dropout)	(None, 4096)	0	
22	<hr/>			
23	fc2 (Dense)	(None, 4096)	16781312	
24	<hr/>			
25	dropout_2 (Dropout)	(None, 4096)	0	
26	<hr/>			
27	predictions (Dense)	(None, 3047)	12483559	
28	<hr/>			
29	Total params: 146,744,103			
30	Trainable params: 146,744,103			
31	Non-trainable params: 0			
32	<hr/>			
33	<hr/>			

Listing 1.1: An excerpt of the VGG16 architecture used for the multi-label classification task.

4 Experiments

In this section, we describe our experimental procedure, model configuration, and a variety of deep CNN architectures that we tried for achieving the multi-label classification task.

Table 4 reports the results of the experiment we conducted throughout the challenge. Because of time constraints, rather than running a grid search for the best hyper-parameter values, we started from a reference configuration, already successfully used in other past works [9,10].

Together with the base architecture used for convolution (CNN arch) we report: (res) the resolution in pixels of the input images of equal height and width, (aug) the data augmentation strategy, (fc layers) the configuration of the final fully-connected stage of the CNN architectures, (do) the dropout value after each fully connected layer, (bs) the batch size used for training, (loss func) the loss function used for optimization, (lr-red) the learning rate reduction strategy (reduction factor/patience/monitored metric). Additionally, we report the best training epoch, based on an early stopping criteria by monitoring the F1 score on the validation set. The last three columns report the F1 scores achieved on the

#	CNN arch	res (px)	aug.	fc layers	do bs	loss func	lr-red.	test1		test2		score
								ep	F1	ep	F1	
1	VGG16	227	none	2x2k	0.5	32	bce	0.2/3/loss	12	0.333	22	0.335
2	VGG16	227	none	2x4k	0.5	32	bce	0.2/3/loss	25	0.346	26	0.336
3	VGG16	227	hflip	2x4k	0.5	32	bce	0.2/5/f1	9	0.3475	9	0.3455
4	VGG16	450	hflip	2x4k	0.5	24	bce	0.2/5/f1	n/a	crash	6	0.3417
5	ResNet50	224	hflip	2x4k	0.5	16	bce	nothing	3	0.3484	3	0.3487
6	DenseNet169	224	none	2x4k	0.5	32	bce	nothing	8	0.3495	10	0.3450
7	DenseNet169	224	hflip	2x4k	0.5	32	bce	nothing	5	0.3500	4	0.3463
8	VGG16	227	hflip	3x4k	0.5	32	bce	0.2/5/f1	13	0.3465	14	0.3433
9	VGG16	227	hflip	2x4k	0.5	48	$\overline{F1} * bce$	0.2/5/f1	11	0.3604	7	0.3606
10	VGG16	227	hflip	2x4k	0.5	48	$\overline{F1} + bce$	0.2/5/f1	14	0.3636	12	0.3632

Table 4: The list of experiments conducted for the challenge.

two internal cross-validation sets and finally on the Aicrowd³ online submission platform.

Other training parameters, common to all configurations are: NAdam optimizer, learning rate = 1e-5, schedule decay 0.9. All images were scaled to the input resolution of the CNN using *nearest* filtering, without any cropping.

In the following, we report on the evolution of our tests and obtained results.

Experiments 1-4: VGG16 baseline We started with (1) a VGG16 architecture, pretrained on ImageNet, with the last two fully connected (FC) layers configured with $n=2048$ nodes, each followed by a dropout layer with the dropout probability p set to 0.5.

(2) We observed an increase in performance by increasing the size of the FC layers to 4096 nodes.

From the first two experiments, it was evident how the loss value (based on binary cross-entropy) could not be effectively used to monitor the validation. The ground truth of each sample, a vector of size 3,047, contains on average about 11 concepts per image (see Section 3.2), and only a few images contain more than 50 concepts. Hence, the ground truth matrix is very sparse. As a consequence, the loss function quickly stabilizes into a plateau, as does the accuracy, which collapses to values above 0.9966 after the first epoch. Hence, to better handle early stopping, we implemented a training-time computation of the F1 score.

(3) A further improvement was observed by applying a 2X data augmentation of the input dataset. Each image is provided to the training procedure both as-it-is and flipped horizontally. At the same time, learning rate reduction was applied by monitoring F1 scores on the validation set, rather than the loss values. However, increasing the learning rate happens only after an overfitting occurs. This configuration led to an online evaluation score of 0.363. Figure 6 shows the evolution of loss values and F1 scores over epochs during model training.

³<https://www.aicrowd.com/challenges/imageclef-2020-caption-concept-detection>

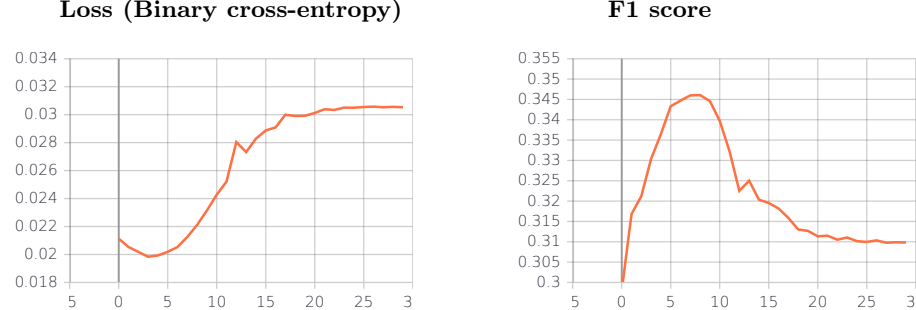


Fig. 6: Plots of the metrics computed on the validation set during training: (left) binary cross-entropy and (right) F1 score. Here, epochs are counted from 0. The best validation results are achieved at epoch 9, then the model starts overfitting.

(4) We tried to improve the performance by increasing the size of input images to 450x450 pixels, which forced a reduction of the batch size to 24. We could not observe any significant improvement in the accuracy, suggesting that higher image resolutions do not provide useful details for label selection in our case.

Experiments 5-7: more powerful CNN architectures By using deeper CNN architectures, we could observe a slight improvement in the test accuracy. Indeed, the ResNet50 architecture (5) led to an F1 score of 0.365 in the online evaluation. The DenseNet169 architecture (6-7) led to higher test values, but the online evaluation was slightly lower (0.360) than the ResNet50 version.

Experiment 8: more layers In order to increase the overall performance, we tried to increase the number of FC layers to 3x4k (8). However, taking as reference the performance of configuration (3), we could not observe a significant improvement by introducing an additional 4k FC layer to the classification stage.

Experiments 9-10: a new loss function To further improve performance, we decided to directly optimize for the F1 score evaluation metric. Notice that the F1 score used in the ImageCLEF challenge is computed as an average F1 over the samples (and not over the labels, as more often found in online code repositories⁴⁵).

We implemented a loss function $\overline{F1} = 1 - sF1$, where $sF1$ is called the “soft F1 score”. The $sF1$ is a differentiable version of the F1 function that computes true positives, false positives, and false negatives as continuous sum of likelihood values, without applying any thresholding to round the probabilities to 0 or 1. The implementation of $\overline{F1}$ is shown in listing 1.2.

⁴<https://towardsdatascience.com/the-unknown-benefits-of-using-a-soft-f1-loss-in-classification-systems-753902c0105d>

⁵<https://www.kaggle.com/rejpalcz/best-loss-function-for-f1-score-metric>

```

1 def loss_1_minus_f1(y_true, y_pred):
2
3     import keras.backend as K
4     import tensorflow as tf
5
6     # The following is not differentiable.
7     # Round the prediction to 0 or 1 (0.5 threshold)
8     # y_pred = K.round(y_pred)
9     # By commenting, we implement what is called soft-F1.
10
11    # Compute precision and recall.
12    tp = K.sum(K.cast(y_true * y_pred, 'float'), axis=-1)
13    # tn = K.sum(K.cast((1 - y_true) * (1 - y_pred), 'float'), axis=-1)
14    fp = K.sum(K.cast((1 - y_true) * y_pred, 'float'), axis=-1)
15    fn = K.sum(K.cast(y_true * (1 - y_pred), 'float'), axis=-1)
16
17    p = tp / (tp + fp + K.epsilon())
18    r = tp / (tp + fn + K.epsilon())
19
20    # Compute F1 and return the loss.
21    f1 = 2 * p * r / (p + r + K.epsilon())
22    f1 = tf.where(tf.is_nan(f1), tf.zeros_like(f1), f1)
23    return 1 - K.mean(f1)

```

Listing 1.2: Python implementation of the *soft-F1* based loss function for the Keras environment with TensorFlow backend.

Experiments using the $\overline{F1}$ loss function could not converge. Likely, the problem is due to the fact that the $\overline{F1}$ loss lies in the range $[0, 1]$. As such, the gradient search space can be abstractly seen as a huge plateau, just below 1.0, with a solitary hole in the middle that quickly converges to the global minimum. At the same level of abstraction, we can visualize the binary cross-entropy *bce* search space as a wide bag, with a large flat surface, just above 0. It is easy to reach the bottom of the bag, i.e., reach a very high binary accuracy due to the sparsity of the labeling, but then we see a very mild slope towards the global minimum at its center.

Our intuition is that by combining (multiplying or adding) $\overline{F1}$ and *bce* results in a search space where $\overline{F1}$ does not affect the identification of inside of the bag, and at the same time helps with the identification of the $\overline{F1}$'s and *bce*'s common global minimum. The implementation of the $\overline{F1} * bce$ loss function is straightforward, as presented in listing 1.3.

(9) An experiment using VGG16 confirms that the loss function $\overline{F1} * bce$ leads to better results with 0.3604/0.3606 on our tests. This is the configuration that performed best in the online submission (0.374).

Further experiments, e.g., using ResNet50, could not be submitted to the challenge due to time constraints. However, (10) an internal test using VGG16 in combination with the $\overline{F1} + bce$ loss function, led to the best performance in our internal evaluation (0.3636/0.3632).

```

1 def loss_1mf1_by_bce(y_true, y_pred):
2     import keras.backend as K
3
4     loss_f1 = loss_1_minus_f1(y_true, y_pred)
5     bce = K.binary_crossentropy(target=y_true, output=y_pred, from_logits=
6                                 False)
7
8     return loss_f1 * bce

```

Listing 1.3: Python implementation of the loss function combining *soft-F1* score with binary cross-entropy.

5 Results and Discussion

The results of our experiments for the ImageCLEFmedical 2020 challenge can be summarized as follows.

The task of concept detection can be modeled as a multi-labeling problem and solved by a transfer learning approach where deep CNNs pretrained on real-world images can be fine-tuned on the target dataset. The multi-labeling is technically addressed by using a sigmoid activation function on the output layer and a label selection by thresholding. A good configuration consists of a VGG16 deep CNN architecture followed by two fully connected layers of 4096 nodes, each followed by a dropout layer with probability p set to 0.5. Augmenting the training set with horizontally flipped images increases accuracy and also reduces the number of epochs needed for training. Increasing the resolution of input images does not prove to be useful, while better results are achieved by substituting the convolution stage with a deeper CNN architecture (ResNet50). We noticed that the learning rate reduction has never helped in improving the results.

Using the standard binary cross-entropy loss function leads to competitive results, which significantly increase when it is combined with a soft-F1 score computation. It is worth noticing that when using solely the soft-F1 score as loss function, the network could not converge and this problem needs further investigation.

In total, we made five online submissions to the challenge. Table 5 presents the F1 scores achieved on the withheld test set and the overall ranking of our team (*iml*) out of 47 successful submissions, as reported by the challenge organizers. In addition, it is worth mentioning that the difference in F1 scores between our best submission and the system that achieved the highest score in the challenge is 0.0195.

6 Conclusion and Future Directions

In this work we have proposed a deep convolutional neural network based approach for concept detection in radiology images. Our best performance (12^{th} position) is achieved by implementing a new loss function whereby we combined

AIcrowd Submission Run	F1 Score	Rank
imageclefmed2020-test-vgg16-f1-bce-nomissing-iml.txt	0.374525478882926	12
imageclefmed2020-test-vgg16-f1-bce-iml.txt	0.374402134956526	13
imageclefmed2020-test-resnet50-iml.txt	0.365168555515581	17
imageclefmed2020-test-vgg16-iml.txt	0.363067945861981	18
imageclefmed2020-test-densenet169-iml.txt	0.360156086299303	19

Table 5: F1 scores for submissions by our team ‘*iml*’.

the widely used binary cross-entropy loss together with a differentiable version of the F1 score evaluation metric.

Still several aspects could be investigated to improve the achieved results. For instance, as we can observe from the CUI distribution plots, there is an imbalance in the dataset. Consequently the model is biased towards predicting the concepts associated with over-represented samples. Our future work will focus on the approaches to combat such type of biases. A straightforward approach would be to undersample the over-represented samples using a query strategy that maximizes informativeness of chosen samples. Such a strategy showed promising results for incremental domain adaptation task in neural machine translation [5].

Furthermore, we did not make use of the existing categorization of the images in 7 sub-sets. A straightforward idea would be to train 7 different models, one per category, and rely on their ensemble for a final global classification result. Alternatively, the class identifier might be used as additional metadata information, concatenated to the images’ internal features representation in the CNN, and fed to a further shallow neural network for improved classification (see [9]). Another idea would be to consider further trends in the integration of vision and language research [8].

References

1. Keras Special Interest Group. Keras. <https://keras.io/>.
2. Kaiming He, Xiangyu Zhang, Shaoqing Ren, and Jian Sun. Deep residual learning for image recognition. In *2016 IEEE Conference on Computer Vision and Pattern Recognition, CVPR 2016, Las Vegas, NV, USA, June 27-30, 2016*, pages 770–778. IEEE Computer Society, 2016.
3. Gao Huang, Zhuang Liu, Laurens van der Maaten, and Kilian Q. Weinberger. Densely connected convolutional networks. In *2017 IEEE Conference on Computer Vision and Pattern Recognition, CVPR 2017, Honolulu, HI, USA, July 21-26, 2017*, pages 2261–2269. IEEE Computer Society, 2017.
4. Bogdan Ionescu, Henning Müller, Renaud Péteri, Asma Ben Abacha, Vivek Datla, Sadid A. Hasan, Dina Demner-Fushman, Serge Kozlovski, Vitali Liauchuk, Yashin Dicente Cid, Vassili Kovalev, Obioma Pelka, Christoph M. Friedrich, Alba García Seco de Herrera, Van-Tu Ninh, Tu-Khiem Le, Liting Zhou, Luca Piras, Michael Riegler, Pål Halvorsen, Minh-Triet Tran, Mathias Lux, Cathal Gurrin,

Duc-Tien Dang-Nguyen, Jon Chamberlain, Adrian Clark, Antonio Campello, Dimitri Fichou, Raul Berari, Paul Brie, Mihai Dogariu, Liviu Daniel Stefan, and Mihai Gabriel Constantin. Overview of the ImageCLEF 2020: Multimedia retrieval in lifelogging, medical, nature, and internet applications. In *Experimental IR Meets Multilinguality, Multimodality, and Interaction*, volume 12260 of *Proceedings of the 11th International Conference of the CLEF Association (CLEF 2020)*, Thessaloniki, Greece, September 22-25 2020. LNCS Lecture Notes in Computer Science, Springer.

5. Marimuthu Kalimuthu, Michael Barz, and Daniel Sonntag. Incremental domain adaptation for neural machine translation in low-resource settings. In Wassim El-Hajj, Lamia Hadrich Belguith, Fethi Bougares, Walid Magdy, and Imed Zitouni, editors, *Proceedings of the Fourth Arabic Natural Language Processing Workshop, WANLP@ACL 2019, Florence, Italy, August 1, 2019*, pages 1–10. Association for Computational Linguistics, 2019.
6. Alex Krizhevsky, Ilya Sutskever, and Geoffrey E Hinton. ImageNet Classification with Deep Convolutional Neural Networks. In F. Pereira, C. J. C. Burges, L. Bottou, and K. Q. Weinberger, editors, *Advances in Neural Information Processing Systems 25*, pages 1097–1105. Curran Associates, Inc., 2012.
7. Martín Abadi, Ashish Agarwal, Paul Barham, Eugene Brevdo, Zhifeng Chen, Craig Citro, Greg S. Corrado, Andy Davis, Jeffrey Dean, Matthieu Devin, Sanjay Ghemawat, Ian Goodfellow, Andrew Harp, Geoffrey Irving, Michael Isard, Yangqing Jia, Rafal Jozefowicz, Lukasz Kaiser, Manjunath Kudlur, Josh Levenberg, Dandelion Mané, Rajat Monga, Sherry Moore, Derek Murray, Chris Olah, Mike Schuster, Jonathon Shlens, Benoit Steiner, Ilya Sutskever, Kunal Talwar, Paul Tucker, Vincent Vanhoucke, Vijay Vasudevan, Fernanda Viégas, Oriol Vinyals, Pete Warden, Martin Wattenberg, Martin Wicke, Yuan Yu, and Xiaoqiang Zheng. *TensorFlow: Large-Scale Machine Learning on Heterogeneous Systems*. 2015.
8. Aditya Mogadala, Marimuthu Kalimuthu, and Dietrich Klakow. Trends in integration of vision and language research: A survey of tasks, datasets, and methods. *CoRR*, abs/1907.09358, 2019.
9. Fabrizio Nunnari, Chirag Bhuvaneshwara, Abraham Obinwanne Ezema, and Daniel Sonntag. A study on the fusion of pixels and patient metadata in CNN-based classification of skin lesion images. In *International IFIP Cross Domain Conference for Machine Learning and Knowledge Extraction (CD-MAKE)*. Springer, August 2020.
10. Fabrizio Nunnari and Daniel Sonntag. A CNN toolbox for skin cancer classification. *arXiv:1908.08187 [cs, eess]*, August 2019. arXiv: 1908.08187.
11. Obioma Pelka, Christoph M Friedrich, Alba García Seco de Herrera, and Henning Müller. Overview of the ImageCLEFmed 2020 concept prediction task: Medical image understanding. In *CLEF2020 Working Notes*, CEUR Workshop Proceedings, Thessaloniki, Greece, September 22-25 2020. CEUR-WS.org.
12. Obioma Pelka, Sven Koitka, Johannes Rückert, Felix Nensa, and Christoph M Friedrich. Radiology objects in context (roco): A multimodal image dataset. In *Intravascular Imaging and Computer Assisted Stenting and Large-Scale Annotation of Biomedical Data and Expert Label Synthesis*, pages 180–189. Springer, 2018.
13. Karen Simonyan and Andrew Zisserman. Very deep convolutional networks for large-scale image recognition. In Yoshua Bengio and Yann LeCun, editors, *3rd International Conference on Learning Representations, ICLR 2015, San Diego, CA, USA, May 7-9, 2015, Conference Track Proceedings*, 2015.

14. Daniel Sonntag. AI in Medicine, Covid-19 and Springer Nature's Open Access Agreement. *KI*, 34(2):123–125, 2020.
15. Daniel Sonntag, Fabrizio Nunnari, and Hans-Jürgen Profitlich. The Skincare project, an interactive deep learning system for differential diagnosis of malignant skin lesions. Technical Report. *CoRR*, abs/2005.09448, 2020.
16. Daniel Sonntag and Hans-Jürgen Profitlich. An architecture of open-source tools to combine textual information extraction, faceted search and information visualisation. *Artif. Intell. Medicine*, 93:13–28, 2019.
17. Daniel Sonntag, Volker Tresp, Sonja Zillner, Alexander Cavallaro, Matthias Hammon, André Reis, Peter A. Fasching, Martin Sedlmayr, Thomas Ganslandt, Hans-Ulrich Prokosch, Klemens Budde, Danilo Schmidt, Carl Hinrichs, Thomas Wittenberg, Philipp Daumke, and Patricia G. Oppelt. The clinical data intelligence project - A smart data initiative. *Informatik Spektrum*, 39(4):290–300, 2016.
18. Grigoris Tsoumakas and Ioannis Katakis. Multi-Label Classification: An Overview. *International Journal of Data Warehousing and Mining*, 3(3):1–13, July 2007.